

XRD and nanoindentation testing of thermo-mechanically processed Ti-29Nb-9Ta-10Zr alloy

I. Cinca¹, A. Nocivin^{2*}, D. Raducanu¹, T. Gloriant³, D. M. Gordin³, I. Dan⁴, A. Caprarescu¹, V. D. Cojocaru¹

¹*POLITEHNICA University of Bucharest, Faculty of Materials Science and Engineering, 060042 Bucharest, Romania*

²*OVIDIUS University of Constanta, Faculty of Mechanical, Industrial and Maritime Engineering, 900527 Constanta, Romania*

³*INSA Rennes, UMR CNRS 6226 SCR/Chimie-Métallurgie, F-35708 Rennes Cedex, France*

⁴*SC R&D Consulting and Services, 023761 Bucharest, Romania*

Received 22 March 2013, received in revised form 6 June 2014, accepted 22 July 2014

Abstract

Ti-Nb-Ta-Zr alloys (TNTZ) represent a new class of biomaterials, due to nontoxic chemical elements and promising combination of high mechanical resistance with low elastic modulus close to the bone elasticity ($E = 20\text{--}40$ GPa). The present paper proposes a particular chemical composition of this β type Ti alloy – Ti-29Nb-9Ta-10Zr (wt.%) with a particular material structure. Structural and mechanical characterization of four distinct alloy conditions corresponding to each TM stage was performed using XRD measurements and also nanoindentation measurements. The obtained results represent a solid base for complex optimization of the alloy's structural characteristics.

Key words: beta titanium alloy, thermo-mechanical processing, XRD spectra, nanoindentation

1. Introduction

Ti-based alloys are often used as implant materials due to their high strength to density ratio, superior biocompatibility and corrosion resistance, high mechanical resistance and low elastic modulus [1, 2].

Even if the elastic modulus of commonly used biocompatible ($\alpha + \beta$)-Ti alloys (100–110 GPa) is much smaller than that of the stainless steel (210 GPa), it remains significantly higher than that of bone tissue with an elastic modulus in the range of 10–40 GPa [3]. This gives rise to the so-called “stress shielding” effect that can cause bone resorption and loosening of implants [4]. This problem can be resolved by using an alloy with an elastic modulus closer to that of the bone. On that direction, there have recently been developed new near- β and metastable- β titanium alloys with low elastic modulus, containing only non-toxic metallic alloying elements such as Nb, Ta, and Zr, etc., with excellent mechanical properties [1, 5]. Zr is added to increase the strength, Ta to improve corrosion resistance

and mechanical performance [6], while Nb is added as a β stabilizing element and for increasing hot workability, too [7]. In that direction, Sakaguchi et al. [8, 9] investigated the elastic modulus of Ti-30Nb-XTa-5Zr alloys as a function of their Ta content: the lowest elastic modulus of 67 GPa is observed for 10 Ta. Thus, the elastic modulus decreases when the Ta content increases up to 10 mass%. On his turn, Niinomi et al. [10] have developed an optimized quaternary Ti-29Nb-13Ta-4.6Zr (wt.%) alloy for which the elastic modulus is around 60 GPa. Malek et al. [11] have investigated the influence of changing Zr and Ta contents on mechanical properties and also on precipitation of secondary phases during ageing treatment for some Ti-Nb-Ta-Zr alloys. Also, Nakai et al. [12] have investigated the possibility of fatigue strength improvement for a particular biomedical β -type Ti-Nb-Ta-Zr alloy while maintaining low Young's modulus through optimizing ω -phase precipitation. On the other hand, Saito et al. [13] have reported that cold working substantially decreases the elastic modulus and increases the

*Corresponding author: tel./fax: +40 241606431; e-mail address: anocivin@univ-ovidius.ro

yield strength of Ti-23Nb-0.7Ta-2Zr-O alloy, though the reasons for this decrease in the elastic modulus have not been discussed in detail. Hao et al. [1] have investigated the influence of α'' martensite on Young's modulus and mechanical properties of forged Ti-29Nb-13Ta-4.6Zr (wt.%) alloy and concluded that the Young's modulus of α'' martensite is comparable with β phase.

With the background research results above, this present investigation proposes a particular chemical composition of this new system of β titanium alloy with no toxic alloying elements – Ti-29Nb-9Ta-10Zr (wt.%) – a TNTZ alloy with a particular route of the applied TM treatment, which included cold deformation, owing the excellent cold workability of β -Ti alloys, that can be utilized to obtain good mechanical properties. Therefore, particular emphasis was laid on measuring the hardness and the elastic modulus of the alloy by nanoindentation technique correlated with the microstructure characteristics analyzed by XRD measurements.

2. Material and methods

2.1. The synthesis and the thermo-mechanical process applied to the Ti-29Nb-9Ta-10Zr alloy

In order to obtain the desired chemical composition of the proposed Ti-based alloy, commercially high purity chemical elements and a FIVE CELES – MP25 furnace had been used. The alloy had been produced by cold crucible induction in levitation melting, under argon protective atmosphere. For a better chemical homogeneity of the final as-cast sample, the ingot was re-melted two times, having in view the significant difference of the melting points of the component elements (Ti – 1660 °C; Nb – 2468 °C; Ta – 2996 °C; Zr – 1855 °C). After this first step of the alloy synthesis process, 4 specimens were prepared from the obtained alloy ingot for 4 different structural conditions (Fig. 1). The as-cast S1 sample represented the initial one. The other three samples corresponded to the next stages of the thermo-mechanical process applied further to the studied alloy.

The sample S2 corresponded to the second stage recorded after the homogenization treatment which was applied to the alloy in order to obtain higher homogeneity. This treatment of homogenization was performed at 950 °C for 6 h, in high vacuum, with final sample air cooling.

Further, the next step of alloy processing was represented by sample S3 obtained after applying a cold-rolling, using a thickness reduction of 60 %.

The final fourth step – sample S4 – corresponded to a heat treatment applied after cold-rolling in order to remove the strain-hardening resulted during cold

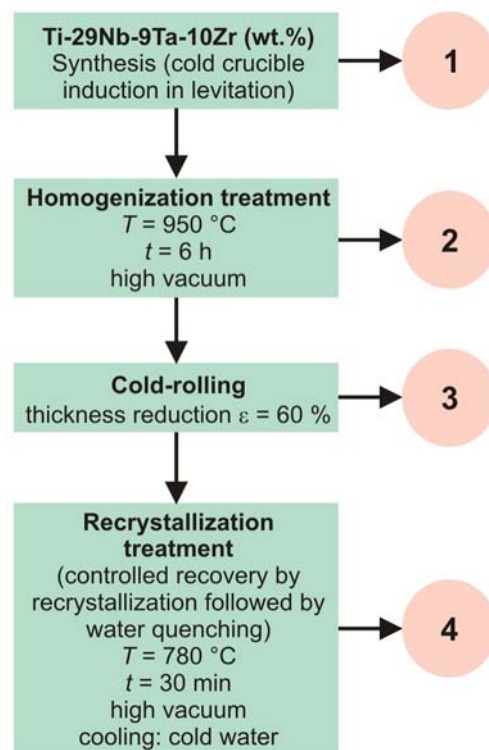


Fig. 1. The route of thermo-mechanical process applied on Ti-29Nb-9Ta-10Zr alloy, with indication of the four distinct investigated sample states.

deformation. This heat treatment was performed at 780 °C for 30 min, in high vacuum, with final sample water quenching in order to obtain a bimodal structure consisting of parent β -Ti phase and temperature-induced α'' -Ti phase.

For a proper understanding of the fourth distinct sample status, subjected to structural investigations, Fig. 1 schematically indicates the route of synthesis and thermo-mechanical processes applied to Ti-29Nb-9Ta-10Zr alloy.

From all fourth-stage samples, other samples were cut away in order to be used for XRD and nanoindentation measurements. The specimens were fixed on specific epoxy resin, abraded with 1200 grit SiC paper, and mechanically polished using 6, 3, 1 μm diamond paste and 0.03 μm colloidal silica. Total removed thickness of the layer was about 150 μm . For the samples subjected to cold rolling, the observation plane was parallel to rolling direction, in the T-L plane.

2.2. XRD measurements

The X-ray diffraction was performed using a Philips PW 3710 diffractometer, with Cu K α ($\lambda = 0.15406 \text{ nm}$). The goal was to determine the phase structure and phase characteristics. For that reason,

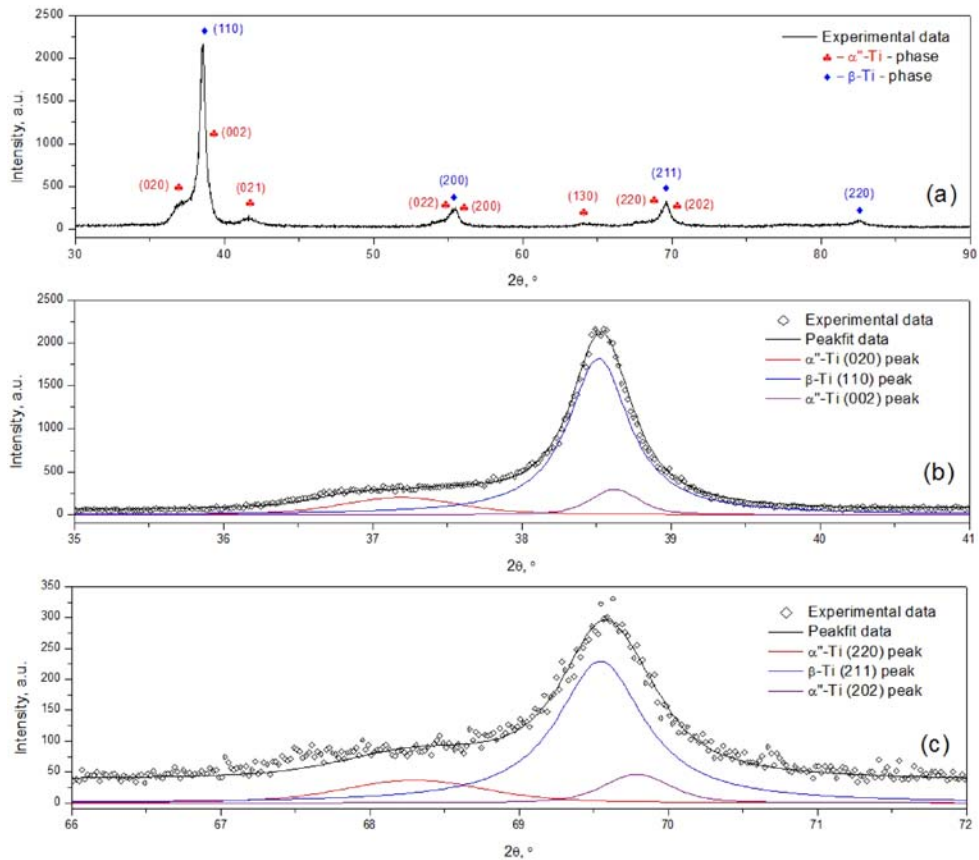


Fig. 2. XRD spectra corresponding to sample S1 of the Ti₂₉Nb-9Ta-10Zr alloy; (a) recorded spectra; (b) detailed zoom $2\theta = (35^\circ\text{--}41^\circ)$; (c) detailed zoom $2\theta = (66^\circ\text{--}72^\circ)$.

all recorded XRD spectra were simulated and fitted. For the XRD spectra simulation the *MAUD v2.33* software package had been used, by which the phase lattice parameters can be calculated. The fitting procedure was performed using the *PeakFit v4.12* software package, in order to determine the position and intensity of each peak, and the peak broadening – FWHM (Full Width at Half Maximum). A pseudo-Voigt diffraction line profile was used in fitting procedure.

2.3. Nanoindentation measurements

The nanoindentation testing of the thermo-mechanical Ti-29Nb-9Ta-10Zr (wt.%) processed alloy was performed by CSM – NHTX S/N: 01-03279 nano-hardness-testers, with a triangular pyramidal diamond indenter (Berkovich, B-I 93), the maximum load being at 100 mN at the load rate 200 mN min⁻¹, and for a constant loading mode.

Indentations were sufficiently spaced so that the indentation behaviour was not affected by the presence of adjacent indentations. The nano-hardness tester was calibrated using glass and fused silica samples.

Within nanoindentation techniques, the CSM instruments (Continuous Stiffness Measurement) allows the indentation hardness, elastic modulus and stiff-

ness to be obtained as a function of depth. Thus, the Instrumented Hardness (H_{IT}) and Instrumented Elastic Modulus (E_{IT}) were estimated using the initial gradient of the load-depth profiles, in conformity with Oliver and Pharr model [14–16]. Vickers microhardness (HV) was also determined. Ten measurements were made on each sample, the maxima and minima were removed and the rest were used in order to obtain average measurement values.

3. Results and discussion

3.1. Results and discussion for XRD measurements

In order to detect the alloy phase components and structural phase characteristics, all recorded XRD spectra (Figs. 2–5) were simulated and fitted, using the *MAUD v2.33* software package, by which the phase lattice parameters have been calculated for all four different alloy stages proposed for study. The fitting procedure was performed using the *PeakFit v4.12* software package, in order to determine the position and intensity of each peak, and the peak broadening.

Figure 2 indicates the XRD profile (experimental

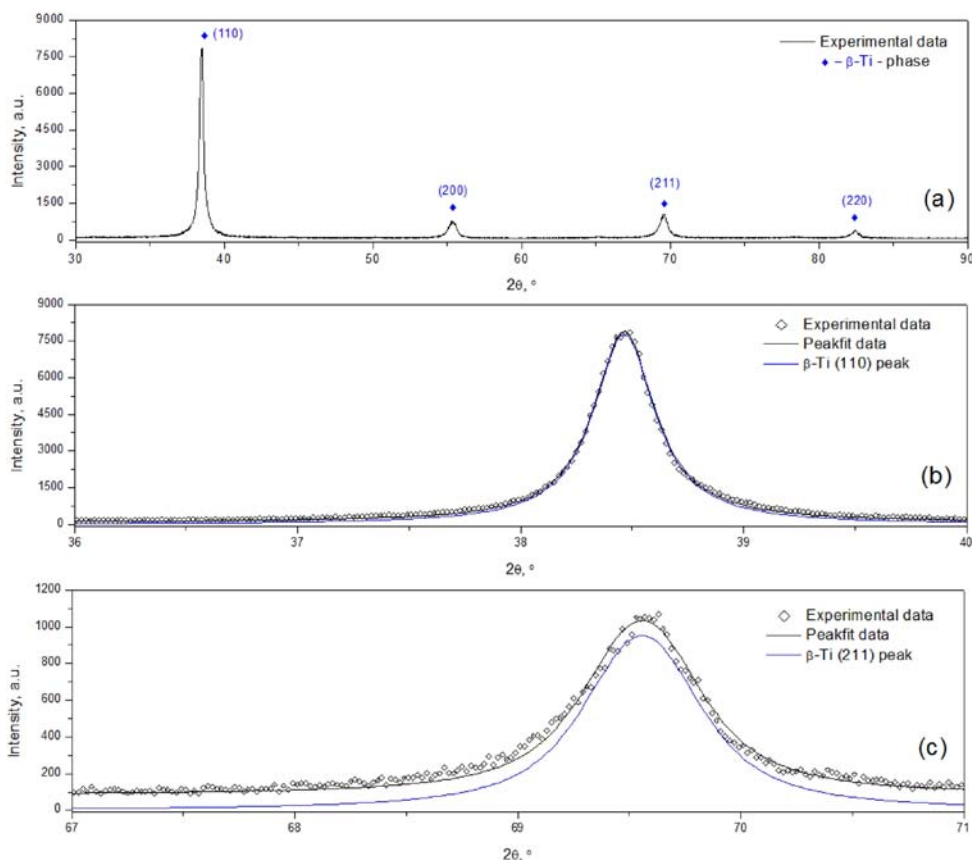


Fig. 3. XRD spectra corresponding to sample S2 of the Ti₂₉Nb-9Ta-10Zr alloy; (a) recorded spectra; (b) detailed zoom $2\theta = (36^\circ\text{--}40^\circ)$; (c) detailed zoom $2\theta = (67^\circ\text{--}71^\circ)$.

data and the peak-fit data) corresponding to as-cast S1 sample of Ti₂₉Nb-9Ta-10Zr (wt.%) alloy, after the initial synthesis process. Figure 2a shows the recorded spectra, Fig. 2b the detailed zoom $2\theta = (35^\circ\text{--}41^\circ)$, while Fig. 2c the detailed zoom $2\theta = (66^\circ\text{--}72^\circ)$. As the dominant phase, the β -Ti phase was identified clearly on the XRD profile (indexed in bcc system – $Im\text{-}3m$, with cell parameter $a_\beta = 0.331$ nm) alongside with α'' -Ti phase (indexed in orthorhombic system – $Cmcm$, with cell parameters $a_{\alpha''} = 0.330$ nm; $b_{\alpha''} = 0.483$ nm and $c_{\alpha''} = 0.466$ nm).

The XRD profile in Fig. 3, corresponding to the alloy from sample S2 after the homogenization treatment, indicates the β -Ti phase peaks only (experimental and peak-fit data also), with the same value of the calculated lattice parameter $a_\beta = 0.331$ nm. This fact confirmed the success of the homogenization treatment by which α'' -Ti martensitic phase is not formed, meaning that, during cooling, the martensitic transformation $\beta \rightarrow \alpha''$ did not take place, due to Martensite Start Temperature (M_s) which was below room temperature. Tang et al. [17], who have studied the phase transformations for the TNTZ alloys system, concluded that by increasing the Nb + Ta + Zr content, the CCT (continuous cooling transformation) curves for transformations with diffusion ($\beta \rightarrow \alpha$ and β

$\rightarrow \omega$) were gradually moving to the right and the temperature M_s was getting down. The consequence is the stabilization of β phase, and the decrease of the critical cooling rates by which the transformations $\beta \rightarrow \alpha$ and $\beta \rightarrow \omega$ were completely suppressed for all cooling conditions. Many other authors agree that the higher the Ta content is, the lower will be the M_s temperature [3, 5, 18–20]. In the case of the sample 2 (after homogenization treatment) the martensitic transformation $\beta \rightarrow \alpha''$ was suppressed and the resulted structure was formed only by β phase, attested by XRD patterns in Fig. 3. These microstructure results are also congruent with the work of Niinomi et al. [10] on the proximate TNTZ alloy (Ti-29Nb-13Ta-4.6Zr (wt.%)).

Figure 4 indicates the XRD profile (experimental data and the peak-fit data again) corresponding to sample S3 of the studied TNTZ alloy, after applying a cold-rolling, using a thickness reduction of 60 %. In that case the XRD profile shows the presence of the both dominant β -Ti phase and less α'' -Ti phase again. The reappearance of α'' -Ti phase can be explained by the deformation-induced phase transformation from bcc metastable β phase to orthorhombic α'' -martensite ($\beta \rightarrow \alpha''$). The ability of these metastable β -Ti alloys to undergo a deformation-induced martensitic transformation during cold-rolling has

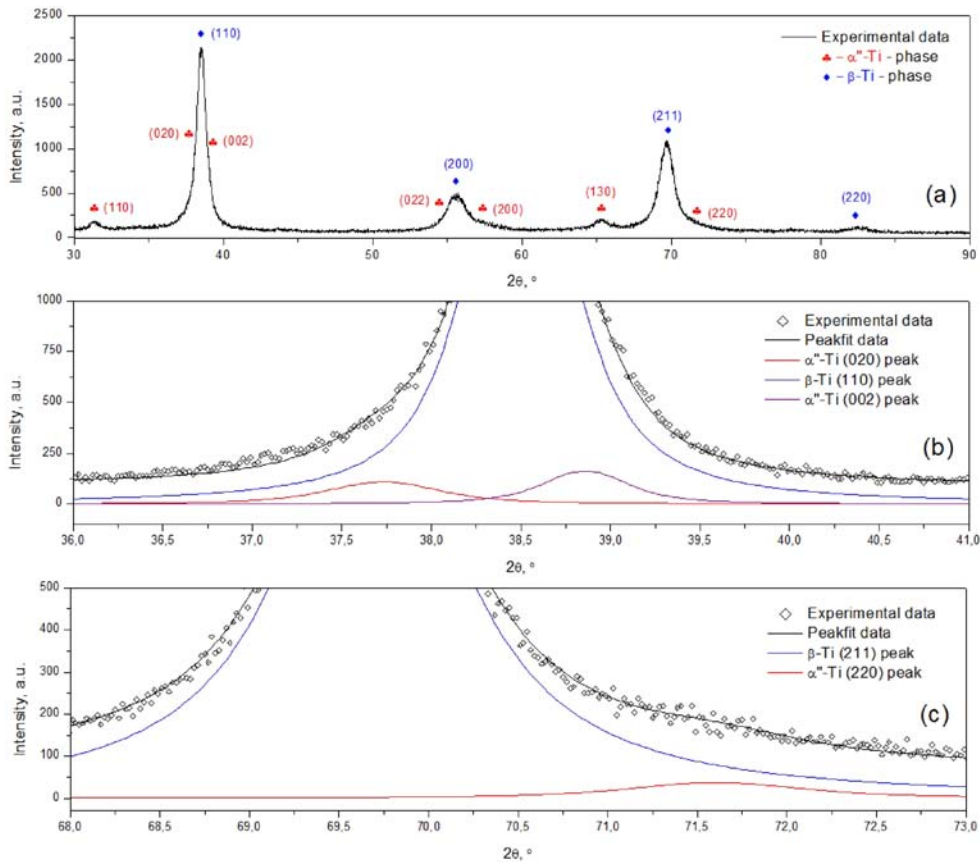


Fig. 4. XRD spectra corresponding to sample S3 of the Ti₂₉Nb-9Ta-10Zr alloy; (a) recorded spectra; (b) detailed zoom $2\theta = (36^\circ\text{--}41^\circ)$; (c) detailed zoom $2\theta = (68^\circ\text{--}73^\circ)$.

already been demonstrated [3, 5]. The advantage of this phenomenon appearing, from biomedical point of view, is an additional decrease of the elastic modulus [5], besides the diminution determined by an increase of the Ta content [3, 5, 21–23]. This aspect will be discussed below with nanoindentation measurement results. The calculation of the lattice parameters for both detected phases was made for this case, too: for the β -Ti phase (indexed in bcc system – $Im\bar{3}m$) $a_\beta = 0.331$ nm and for α'' -Ti phase (indexed in orthorhombic system – $Cmcm$) $a_{\alpha''} = 0.323$ nm, $b_{\alpha''} = 0.476$ nm and $c_{\alpha''} = 0.466$ nm.

The XRD profile in Fig. 5 (experimental and peakfit data on normal and detailed zoom) determined for the studied TNTZ alloy from sample S4, corresponds to heat treatment performed at $780^\circ\text{C}/30$ min/high vacuum, with final sample water quenching. The XRD patterns indicate the presence of both β -Ti and α'' -Ti phases, but with more accentuated peaks for α'' -Ti phase (sharp and strait), compared to the case of the cold rolled sample with more splayed and broadened peaks. These particular characteristics are more evidently visible on detailed zoom from Figs. 5b,c, compared to Figs. 4b,c. This attests a more evident quantity of α'' -Ti phase, due to martensitic transformation $\beta \rightarrow \alpha''$. The unit cell parameters corresponding to

detected phases have been indexed as follows: for the β -Ti phase (indexed in bcc system – $Im\bar{3}m$) $a_\beta = 0.330$ nm; for α'' -Ti phase (indexed in orthorhombic system – $Cmcm$) $a_{\alpha''} = 0.330$ nm; $b_{\alpha''} = 0.477$ nm and $c_{\alpha''} = 0.467$ nm.

Comparing all XRD profiles indicated in Figs. 2–5, it can be observed that regarding the dominant β phase peak intensities, the $(110)_\beta$ peak is constantly the strongest among the β planes in all samples. On the other hand, the $(211)_\beta$ peak became suddenly stronger for sample S3 (cold rolling) and S4 (heat treated) when compared to S1 and S2 samples. These results indicate that the texture is changed by cold rolling: the common rolling textures of strong $\{001\}_\beta$ $\langle 110 \rangle_\beta$ and weak $\{211\}_\beta$ $\langle 110 \rangle_\beta$ for body-centered-cubic (bcc) metals were formed by cold rolling and were even more accentuated by subsequent heat treatment.

It is necessary to remember that there exists a specific lattice correspondence between α'' and β phases as shown in [24], from which it can be observed that α'' [100], α'' [010], and α'' [001] are parallel to β [100], β [011], and β [011], respectively. According to present calculated cell parameters it can be observed that $\sqrt{2}a_\beta = b_{\alpha''} = 0.476$ nm for the samples S3 and S4, and, in addition, $a_\beta = a_{\alpha''} = 0.330$ nm

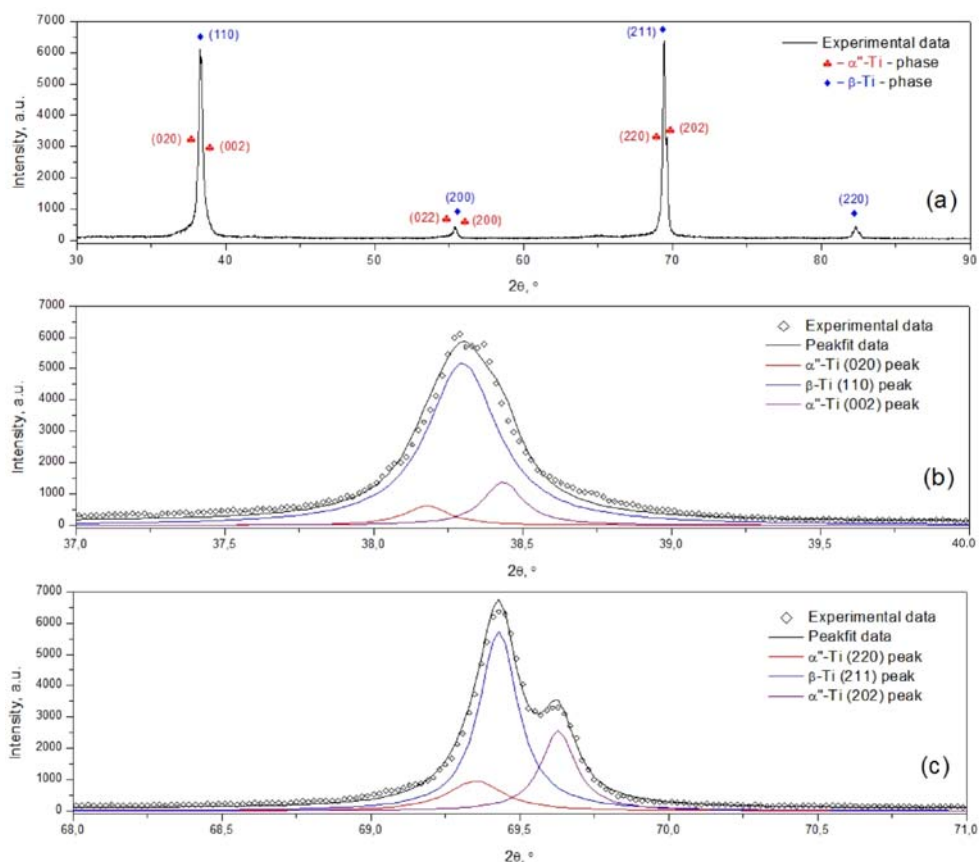


Fig. 5. XRD spectra corresponding to sample S4 of the Ti₂₉Nb-9Ta-10Zr alloy; (a) recorded spectra; (b) detailed zoom $2\theta = (37^\circ\text{--}40^\circ)$; (c) detailed zoom $2\theta = (68^\circ\text{--}71^\circ)$.

for the sample S4. The decrease in length from $b_{\alpha''} = 0.483$ nm (for the S1: as-cast) to $b_{\alpha''} = 0.476$ nm (for the S3: cold rolled and S4: heat treated) until the relations $\sqrt{2}a_{\beta} = b_{\alpha''}$ and $a_{\beta} = a_{\alpha''}$ become valid, may signalize possible special behaviour of presented alloy in cold-rolled or heat treated status (such as negative thermal expansion or even shape memory behaviour), like it had been mentioned in [24] for a TNTZ alloy with closer chemical composition. The stress-induced martensitic transformation and texture changing are possibly the key factors opening special behaviour of presented TNTZ alloys. However, the experimental evidence will be elucidated more clearly by the further crystallographic experiments in future studies.

3.2. Results and discussion for nanoindentation measurements

This part of the present work aims to study the nanoindentation response of the studied TNTZ alloy subjected to different TM treatments. Attempts have been made to estimate the fractional recoverable deformation energy from the load-displacement profile with the aim to assess the structural modifications by heat treatment at nanostructural scale.

Nanoindentation is a technique for determining

both the elastic and plastic properties of the materials at a nanoscale level in a single experiment where no special sample preparation is required (however, a good surface finish is needed). In nanoindentation, the indentation process is continuously monitored with respect to force, displacement and time. The nanoindentation technique should give accurate estimation of the elastic modulus for single-phase materials or for multiphase materials with very fine precipitates distributed homogeneously in the matrix.

As a result of the nanoindentation measurements from this present work, Fig. 6a presents in the beginning a typical aspect of a loading – unloading nanoindentation curve, while Fig. 6b presents the loading – unloading nanoindentation curves obtained after nanoindentation measurements applied on four distinct stages of the studied TNTZ alloy. It can be observed that the obtained four curves are slowly slipped to the right to an increased depth of nanoindentation, from sample S1 to sample S4, respectively.

By processing the obtained specific areas from Fig. 6b, corresponding to characteristic energies for the studied alloy in the four structural stages, the variation of these characteristic energies has been obtained, indicated in Fig. 7: the variation of the plastic energy (W_p) – Fig. 7a; the variation of the elastic en-

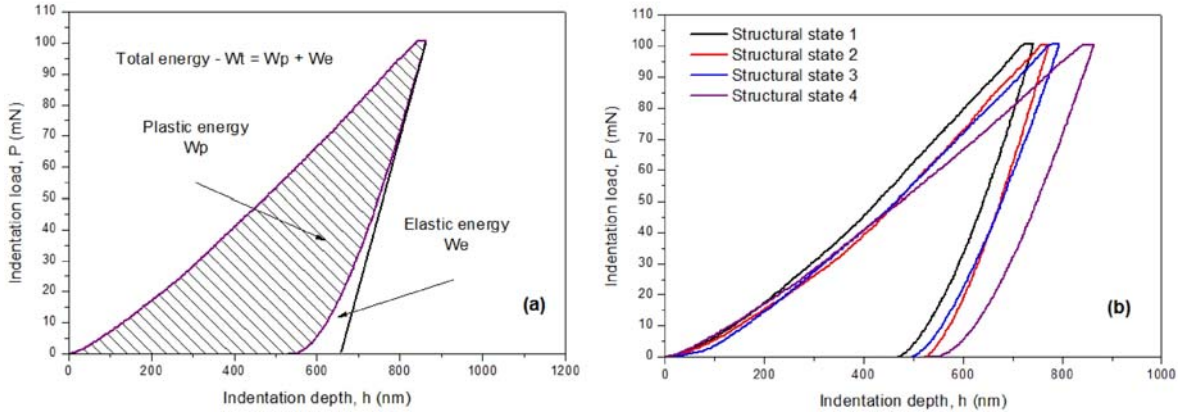


Fig. 6. Load – indentation depth curves of TM processed Ti-29Nb-9Ta-10Zr alloy; (a) typical aspect of a loading – unloading nanoindentation curve; (b) loading – unloading nanoindentation curves of TM processed Ti-29Nb-9Ta-10Zr alloy.

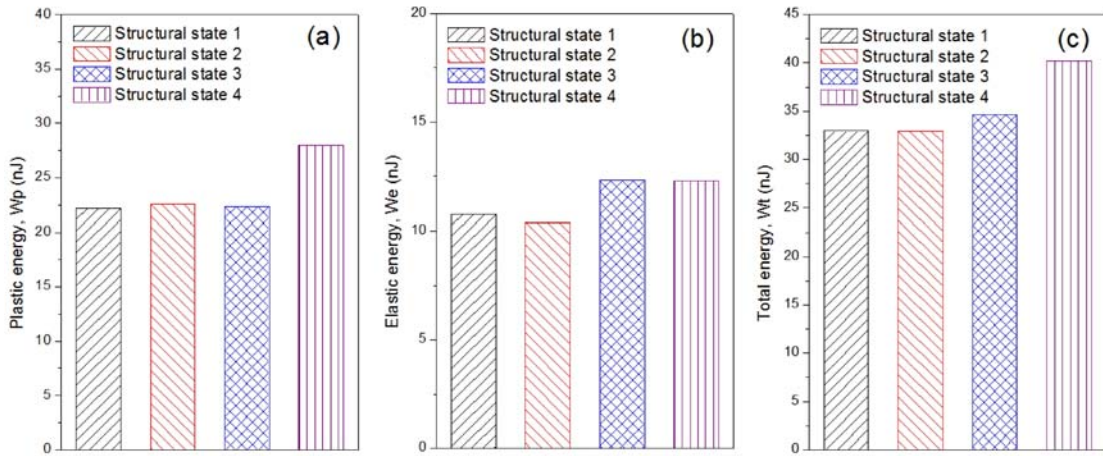


Fig. 7. Variation of the characteristic energy for TM processed Ti-29Nb-9Ta-10Zr alloy: (a) variation of plastic energy (W_p); (b) variation of elastic energy (W_e); (c) variation of total energy (W_t).

ergy (W_e) – Fig. 7b; the variation of the total energy (W_t) – Fig. 7c.

Using the load – depth profiles (the P - h curves) from Fig. 6b and the Oliver and Pharr analysis [14, 15, 25], Fig. 8 indicates the calculated nanoindentation parameters for the studied alloy: the variation of Instrumented Elastic Modulus (E_{IT}) – Fig. 8a; the variation of Instrumented Hardness (H_{IT}) – Fig. 8b; the variation of Vickers microhardness (HV) – Fig. 8c.

From Fig. 7 it can be observed that, for the sample S1 (as-cast sample) and S2 (homogenized status), the variation level of the plastic, elastic and total energy rests unchanged, even if for the sample S2 a homogenization treatment has been performed. Even if the levels of the characteristic energies variations (W_p , W_e and W_t) are similar for the samples S1 and S2, increased values have been determined there for the instrumented elastic modulus E_{IT} , for the instrumented hardness H_{IT} and respectively, for the microhardness HV (Fig. 8), in the case of S2 compared to S1. This fact is due to the disappearance of α'' phase from β

matrix after the homogenization treatment applied on S2. It is well known that the Young's modulus of a dual-phase alloy is mainly determined by modulus of each individual phase and by their volume fractions as well. Therefore, the Young's modulus changes with the type of the phases existing in the alloy [1, 23, 30, 31]. Initially, Han et al. [1] in 2002, reported that the Young's modulus of α'' martensite is comparable with those of β phase. After that, few years later, the contrary had been demonstrated – that there were significant differences in phase modulus: the β -phase had the lowest modulus among all possible phases in most Ti-based alloys, while the ω phase had the highest Young's modulus, and the martensite α'' had a middle value between β and ω phases, but a lower modulus than the martensite α' -phase [23, 30, 31]. In that context, for present studied alloy, due to the disappearance of α'' phase from β matrix after the homogenization treatment applied on S2, the obtained results for the sample S2 can be explained compared to sample S1 presented in Fig. 8.

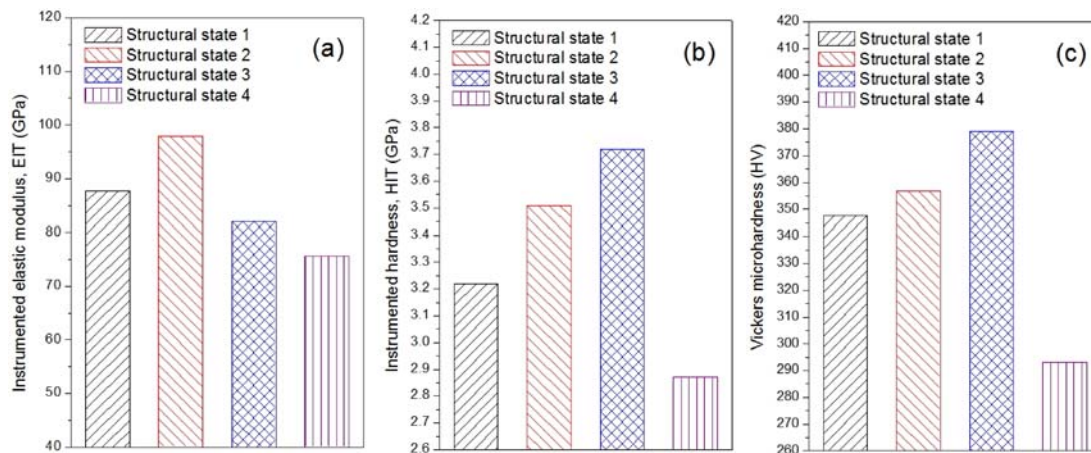


Fig. 8. Calculated nanoindentation parameters of TM processed Ti-29Nb-9Ta-10Zr alloy: (a) variation of Instrumented Elastic Modulus (E_{IT}); (b) variation of Instrumented Hardness (H_{IT}); (c) variation of Vickers microhardness (HV).

The most promising results had been obtained for the sample S3 (cold-rolled) as well as for S4 (heat treatment), for which a significant decrease of the instrumented elastic modulus (EIT) had been registered, compared to S2 (from 98 to 80 GPa for the S3, and respectively to 74 GPa for the S4; see in Fig. 8a). For the sample S3, the instrumented hardness (HIT) and microhardness (HV) had the highest values of all samples, because of the cold-rolled status and the stress-induced martensitic transformation $\beta \rightarrow \alpha''$. Instead of it, sample 4 had lower values for the instrumented hardness (HIT) and microhardness (HV) (Figs. 8b,c) because of the strain softening heat treatment. The cold-rolling-induced elastic modulus decreasing had already been reported [24, 26] due to the proper mechanisms of cold rolling, such as: 1. dislocations slipping; 2. deformation twins, and most important 3. α'' -martensite phase transformation induced by cold rolling [27–29]. The decrease of the elastic modulus caused by deformation is in agreement with the alloy structural evolution observed by XRD measurements and above discussed, allotted to the formation of a $(200)_{\alpha''}/[010]_{\alpha''}$ texture of the α'' phase and to the crystallographic anisotropy of the α'' phase, but also to the formation of the strong rolling texture $\{001\}_{\beta}$ $\langle 110 \rangle_{\beta}$ for the β phase. These results are in accordance with [32, 33] which report that the Young's modulus decreases gradually with the increase of cold reduction due to highly dense defects (vacancies, grain and sub-grain boundaries) and to the $\langle 110 \rangle_{\beta}$ textures along rolling direction formed during cold deformation.

In addition, it must be taken into account that the cold rolled microstructure is strongly influenced by a high density of dislocations and a considerable volume of stress-induced α'' . The deformation defects caused during cold rolling increase the yield strength of β phase, which also enhances the resistance of a martensite transformation. But, due to the fact that by cold-rolling the cell parameters corresponding to α''

and β phases become inter-associated ($\sqrt{2}a_{\beta} = b_{\alpha''}$ and $a_{\beta} = a_{\alpha''}$), it can be signaled that beside the decrease of the elastic modulus the cold-rolling can also open a special alloy behaviour presumed above.

As mentioned in the above introduction, for biomaterials used for load bearing applications, like the presently studied TNTZ alloy, the elastic modulus represents an important parameter. Because of the stiffness mismatch between implant material and surrounding bone causes bone “stress shielding”, higher Young's modulus of the implant will result in a greater amount of bone loss, bone fracture and loss of bone interface. That is the reason why present results (80 GPa for cold-rolling and 74 GPa for recrystallized samples) of measured elastic modulus are very promising because of their approach to bone elasticity (around 40 GPa), compared to higher (110–120 GPa) values, generally corresponding to far-used $(\alpha + \beta)$ -Ti alloys. Present obtained results are situated in actual trend of intensive research of the possibility to optimize the balance of mechanical properties for this very promising non-toxic TNTZ alloys: decreasing the elastic modulus as much as possible, but keeping an increased tensile strength.

4. Conclusions

A particular non-toxic β -Ti-based alloy (Ti-29Nb-9Ta-10Zr wt.%) had been studied performing structural characterization by XRD measurements, and mechanical properties characterization by nanoindentation measurements. Different sets of conclusions can be deduced from this study.

1. For detecting the alloy phase components and phase structural characteristics, all recorded XRD spectra (for sample S1 – as-cast; for sample S2 – homogenized; for sample S3 – cold rolled; for sample S4 – recrystallized) were simulated and fitted, using

the *MAUD v2.33* software package, through which the phase lattice parameters were calculated, and also the *PeakFit v4.12* software package, through which the position and intensity of each peak had been determined, and the peak broadening.

2. Regarding the dominant β phase peaks from XRD profiles, the $(110)_\beta$ peak was constantly the strongest among the β planes in all samples. The $(211)_\beta$ peak became suddenly stronger for sample S3 and S4 compared to S1 and S2 samples, indicating that the texture was changed by cold rolling: the common rolling textures of strong $\{001\}_\beta$ $\langle 110 \rangle_\beta$ and weak $\{211\}_\beta$ $\langle 110 \rangle_\beta$ for bcc metals were formed by cold rolling and were even more accentuated by subsequent controlled recovery.

3. By applying cold-rolling, using a thickness reduction of 60 %, the transformation $\beta \rightarrow \alpha''$ occurred, a deformation-induced phase transformation from bcc metastable β phase to orthorhombic α'' martensite. The result of this transformation is the diminution of the elastic modulus closer to that of human bone.

4. Using the load-depth profiles (the P - h curves) obtained by nanoindentation measurements, and also the Oliver and Pharr analysis, the nanoindentation parameters for all stages of the studied alloy had been calculated: the variation of Instrumented Elastic Modulus (E_{IT}); the variation of Instrumented Hardness (H_{IT}); the variation of Vickers microhardness (HV).

5. The most promising results had been obtained for the sample S3 (cold-rolled) as well as for S4 (heat treated), for which a significant decrease of the instrumented elastic modulus was registered – E_{IT} compared to homogenized status of the alloy (from 98 to 80 GPa – for the S3, and respectively, to 74 GPa – for the S4). For the sample S3, the instrumented hardness (HIT) and microhardness (HV) had the highest values of all samples, because of the cold-rolled status and the stress-induced martensitic transformation $\beta \rightarrow \alpha''$. Instead of it, sample 4 has the lower values for the instrumented hardness (HIT) and microhardness (HV) because of the strain softening heat treatment. These results (80 GPa for cold-rolling and 74 GPa for heat treated samples) of measured elastic modulus are very promising because of the approach to the bone elasticity (around 40 GPa), compared to higher (110–120 GPa) values, generally corresponding to far-used ($\alpha + \beta$)-Ti alloys. The stress-induced martensitic transformation and texture changing are possibly the key factors opening special behaviours of present TNTZ alloys. However, the experimental evidence will be elucidated more clearly by further crystallographic experiments in future studies.

Acknowledgement

This work was supported by a grant of the Romanian National Authority for Scientific Research, CCCDI – UE-

FISCDI, project number MNT-7-075/2013 “Functionalized Super-Elastic Alloys for Load-Bearing Implants”.

References

- [1] Hao, Y. L., Niinomi, M., Kuroda, D., Fukunaga, F., Zhou, Y. L., Yang, R., Suzuki, A.: *Metall Mater Trans A*, 33, 2002, p. 3137. doi:10.1007/s11661-002-0299-7
- [2] Velten, D., Schenk-Meuser, K., Biehl, V., Duschner, H., Breme, J.: *Zeitsch Metallkum*, 6, 2003, p. 667. doi:10.3139/146.030668
- [3] Majumdar, P., Singh, S. B., Chakraborty, M.: *Mater Sci Eng A*, 489, 2008, p. 419. doi:10.1016/j.msea.2007.12.029
- [4] Banerjee, R., Nag, S., Stechschulte, J., Fraser, H. L.: *Biomater*, 25, 2004, p. 3413. doi:10.1016/j.biomaterials.2003.10.041
- [5] Laheurte, P., Prima, F., Eberhardt, A., Gloriant, T., Wary, M., Patoor, E.: *J Mech Behav Biomed Mater*, 3, 2010, p. 565. doi:10.1016/j.jmbbm.2010.07.001
- [6] Nag, S., Banerjee, R., Fraser, H. L.: *Acta Biomater*, 3, 2007, p. 369. doi:10.1016/j.actbio.2006.08.005
- [7] Afonso, C. R. M., Ferrandini, P. L., Ramirez, A. J., Caram, R.: *Acta Biomater*, 6, 2010, p. 1625. doi:10.1016/j.actbio.2009.11.010
- [8] Sakaguchi, N., Niinomi, M., Akahori, T., Takeda, J., Toda, H.: *Mater Sci Eng C*, 25, 2005, p. 363. doi:10.1016/j.msec.2004.12.014
- [9] Sakaguchi, N., Niinomi, M., Akahori, T.: *Mater Trans*, 45, 2004, p. 1113. doi:10.2320/matertrans.45.1113
- [10] Niinomi, M., Akahori, T., Katsura, S., Yamauchi, K., Ogawa, M.: *Mater Sci Eng C*, 27, 2007, p. 154. doi:10.1016/j.msec.2006.04.008
- [11] Malek, J., Hnilica, F., Vesely, J., Smola, B., Bartakova, S., Vanek, J.: *Mater Design*, 35, 2012, p. 731. doi:10.1016/j.matdes.2011.10.030
- [12] Nakai, M., Niinomi, M., Oneda, T.: *Metall Mater Trans A*, 43, 2012, p. 294. doi:10.1007/s11661-011-0860-3
- [13] Saito, T., Furuta, T., Hwang, J. H., Kuramoto, S., Nishino, K., Suzuki, N., Chen, R., Yamada, A., Ito, K., Seno, Y., Nonaka, T., Ikehata, H., Nagasako, N., Iwamoto, C., Ikuhara, Y., Sakuma, T.: *Science*, 300, 2003, p. 464. doi:10.1126/science.1081957
- [14] Oliver, W. C., Pharr, G. M.: *J Mater Res*, 7, 1992, p. 1564. doi:10.1557/JMR.1992.1564
- [15] Oliver, W. C., Pharr, G. M.: *J Mater Res*, 19, 2004, p. 3. doi:10.1557/jmr.2004.19.1.3
- [16] Fischer-Cripps, A. C.: *Surf Coat Technol*, 200, 2006, p. 4153. doi:10.1016/j.surfcoat.2005.03.018
- [17] Tang, X., Ahmed, T., Rack, H. J.: *J Mater Sci*, 35, 2000, p. 1805. doi:10.1016/10.1023/A:1004792922155
- [18] Buenconsejo, P. J. S., Kim, H. Y., Hosoda, H., Miyazaki, S.: *Acta Mater*, 57, 2009, p. 1068. doi:10.1016/j.actamat.2008.10.041
- [19] Kim, H. Y., Hashimoto, S., Kim, J., Imamura, T., Hosoda, H., Miyazaki, S.: *Mater Sci Eng A*, 417, 2006, p. 120. doi:10.1016/j.msea.2005.10.065
- [20] Miyazaki, S., Kim, H. Y., Hosoda, H.: *Mater Sci Eng A*, 438–440, 2006, p. 18. doi:10.1016/j.msea.2006.02.054
- [21] Niinomi, M.: *J Mech Behav Biomed Mater*, 1, 2008, p. 30. doi:10.1016/j.jmbbm.2007.07.001

- [22] Laheurte, P., Eberhardt, A., Philippe, M. J.: *Mater Sci Eng A*, 396, 2005, p. 223.
[doi:10.1016/j.msea.2005.01.022](https://doi.org/10.1016/j.msea.2005.01.022)
- [23] AbdelHady, M., Henoshita, K., Morinaga, M.: *Scr Mater*, 55, 2006, p. 477.
[doi:10.1016/j.scriptamat.2006.04.022](https://doi.org/10.1016/j.scriptamat.2006.04.022)
- [24] Nakai, M., Niinomi, M., Akahori, T., Tsutsumi, H., Feng, X., Ogawa, M.: *Mater Trans*, 50, 2009, p. 423.
[doi:10.2320/matertrans.MRP2008380](https://doi.org/10.2320/matertrans.MRP2008380)
- [25] Sinha, A., Datta, S., Chattopadhyay, P. P.: *Inter J Nanosci*, 10, 2011, p. 955.
[doi:10.1142/S0219581X1100871X](https://doi.org/10.1142/S0219581X1100871X)
- [26] Ikeda, M., Komatsu, S. Y., Sowa, I., Niinomi, M.: *Metall Mater Trans A*, 2002, 33, 487.
[doi:10.1007/s11661-002-0110-9](https://doi.org/10.1007/s11661-002-0110-9)
- [27] Wang, L., Lu, W., Qin, J., Zhang, F., Zhang, D.: *Mater Charact*, 61, 2010, p. 535.
[doi:10.1016/j.matchar.2010.02.009](https://doi.org/10.1016/j.matchar.2010.02.009)
- [28] Wang, L., Lu, W., Qin, J., Zhang, F., Zhang, D.: *Mater Sci Eng A*, 490, 2008, p. 421.
[doi:10.1016/j.msea.2008.03.003](https://doi.org/10.1016/j.msea.2008.03.003)
- [29] Niinomi, M., Akahori, T., Nakai, M.: *Mater Sci Eng C*, 28, 2008, p. 406. [doi:10.1016/j.msec.2007.04.028](https://doi.org/10.1016/j.msec.2007.04.028)
- [30] Matlakhova, L. A., Matlakhova, A. N., Monteiro, S. N., Fedotov, S. G., Goncharenko, B. A.: *Mater. Sci. Eng. A*, 393, 2005, p. 320.
[doi:10.1016/j.msea.2004.11.021](https://doi.org/10.1016/j.msea.2004.11.021)
- [31] Zhou, Y. L., Niinomi, M., Akahori, T.: *Mater. Sci. Eng. A*, 371, 2004, p. 283.
[doi:10.1016/j.msea.2003.12.011](https://doi.org/10.1016/j.msea.2003.12.011)
- [32] Ma, Y. Q., Yang, S. Y., Jin, W. J., Wang, Y. N., Wang, C. P., Liu, X. J.: *Trans Nonferr Met Soc China*, 21, 2011, p. 287. [doi:10.1016/S1003-6326\(11\)60711-5](https://doi.org/10.1016/S1003-6326(11)60711-5)
- [33] Wang, Y., Zhao, J., Dai, S., Chen, F., Yu, X., Zhang, Y.: *J Mech Behav Biomed Mater*, 27, 2013, p. 33.
[doi:10.1016/j.jmbbm.2013.06.006](https://doi.org/10.1016/j.jmbbm.2013.06.006)